Time-resolved imaging of microquasar jets

Theodoros Smponias[1]

PO box 5, PO 2, Ioannina, Greece

Abstract

Particle emission from simulated twin microquasar jets is calculated in a unified manner. A program suite assembled around model data produces synthetic images and spectra, directly comparable to potential observations by contemporary arrays. The model is capable of describing a multitude of system geometries, incorporating increasing levels of realism, depending on the needs and on available computational resources. As an application, the modelling process is applied to a typical microquasar, which is synthetically observed from three different angles and with different imaging geometries.

Keywords:

ISM: jets and outflows, stars: winds-outflows, stars: flare, radiation mechanisms: general, methods: numerical

2010 MSC: 85-08

1. Introduction

Microquasars (MQ) comprise a binary stellar system where a main sequence star orbits a compact object, either a neutron star or a black hole. Matter from the star accretes onto the collapsed stellar remnant, resulting to the production of twin relativistic jets, pointing in opposite directions [1]. Those jets emit over a broad spectrum, from radio to very high energy (VHE) γ-rays and neutrinos [2],[3],[4],[5], [6]).

*Corresponding author

Email address: t.smponias@hushmail.com (Theodoros Smponias)

As mentioned in [2], apparent superluminal motion in certain MQ indicate the presence of bulk hadron flows in the jets. The assumption of equipartition [5], leads to high magnetic field estimates for the jet [7]. This, coupled with the fluid approximation for the jet matter, due to the presence of tangled magnetic fields [8], [9], allows the magneto-hydrodynamic (MHD) approximation for the jets. A toroidal magnetic field component may retain jet collimation over considerable distances along its path [7] [10].

In this paper, the production of VHE neutrinos from generic MQ jets is modelleded, using the method of dynamic and radiative relativistic MHD simulation. The paper is organized as follows:

SOS THIS LIST FOR ZE PAPER!

.jets sims, analytical HTWIN JET, precession (spaniards 2019 paper, blundell 2011 paper , both on precession)

. visuals RLOS2, synthetic image,

. neutrino emission (ref gamma ray emission) REFS from GRB also. ALSO ref 2019 reynoso, also TR13/11, PS01, ERRROR FROM TR13 correct in ARGS09, COUPLINg, accel, etc.

.RESULTS

WHOLE JET LIGHT Curves (SED's over time), SED (many E), also from st.state jet!

SOS state the time stamp of the jet images, i.e. ze tmin param SOS

PARAM files put into folders their main stuff! (cant do all of them!) TABLE AT END! MOVE INTO RESUTLS SECTION!

ALSO interim quantities F,Q,U,Qneutrino vs Reynoso 19 and ARGS09 papers. SOS reproduce, do include some normalization!

****

SHORT INTRO, 1 page mn, 2-pgs this format! NO MOAR! SOS!

SOS MAX 10 PAGES IN THIS FORMAT, i.e. equivalent of 4-5 pages MAX in MN-style format! NO MOAR SOS!!! kepp it BELOW 10 pgs HERE!!! SOS! 240420

2. Theoretical setup

In our generic MQ model, an accretion disk is assumed around the compact object [11]. The twin jets emanate from the vicinity of the collapsed star, collimated by a toroidal magnetic field component. The kinetic power of the twin model jets is L_k=2×2.64 × 10^{38} (see Appendix). [5] argue a 10 percent Eddington luminocity jet power, leading to L_k=10^{38} ergs^{-1} for a 10 M_{solar} black hole, which is compatible with our simulation. Furthermore, the same authors argue $\frac{L_p}{L_e} \simeq 100$ or ≃1, but in our case we shall adopt the former hypothesis, favouring protons. Equipartition means $\rho_k = \rho_B$, therefore $B(z) = \sqrt{8\pi\rho_z}$. Rieger et al (7,19) 2020 review SOS Find that multi-author ref! : SOS EQUIPARTITION CALC FROM NOTE BOOK PUT HERE. ALSO, JET CALC FROM NOTEBOOK PUT HERE SOS indeed get that notebook fron back home, or its scans SUPERSOS

2.1. Non-thermal proton density

Neutrino emission from the jets is taken to originate from proton-proton interaction between a distribution of hot (fast) protons and cold (bulk flow) protons [2, 4, 5, 6**?** **?**]. Some of the bulk protons get accelerated at shock fronts, saccording to first order Fermi acceleration mechanism. We have ([12], [8], [9])

$$t_{acc}^{-1} \simeq \eta \frac{ceB}{E_p}, \tag{1}$$

where B is the magnetic field and E_p the proton energy (e being the proton charge and c the speed of light. $\eta = 0.1$ represents an acceleration efficiency parameter, assuming efficient acceleration in moderately relativistic shocks in the vicinity of the jet base [12].

In the present work, we assume a power-law distribution of the form $N_p = N_0 E^{-\alpha}$, with $\alpha \approx 2$ [**?**], or perhaps a variable α [6], where α is the proton spectral index in the local jet cell matter frame.

As an approximation, the aforementioned hot proton distribution is taken to be isotropic in the jet frame, assuming the scattering length l_{sc} is less than the radiative length, l_r, a hypothesis backed by the nature of diffuse shock acceleration [13].

2.2. Jet frame anisotropy

A NOTE ON ASSUMED JET-FRAME ISOTROPY EMISSION.

Based on [13] we note the description of a jet-frame isotropic emission: fast (hot-jet) protons and electrons distro must be isotropic in jet-frame, in order to emit photons isotropically in said frame. Also, l_{sc} must be smaller than l_r, for fast particles' distros, in order for their emission to be isotropic. For protons accelerated at diffuse scocks, this goes by definition, since at shocks it has to preserve, after every bounce, at least some E, therefore l_{sc} is clearly less than l_r, else it wouldnt have any E left after each bounce!

But, there is some anisotropy inherent in every distro, depending on the circumstances. Still, [13] provide a solid justification and description for the jet-frame isotropy assumption [9]

180520 read rieger 2019, also abstract of 2019 long particle accel review: dig that up! SOS coupling of RMHD and radiation, l_{sc} vs lrad, fokker planck, velocity shear acceleration, etc. also tangled B field. Our coupling from [5].

3. Neutrino emission calculations

3.1. Hot proton energy loss mechanisms

SOS HERE REFER TO LOSS MECHANISMS SOS 280420 SOS

Following [**?**], [5], and [6], we incorporate mainly synchrotron and adiabatic energy loss mechanisms.

SOS now loss mechanisms from nemiss 210321

$$t_\pi = t_{\pi 0}\Gamma_\pi + t_{esc} \tag{2}$$

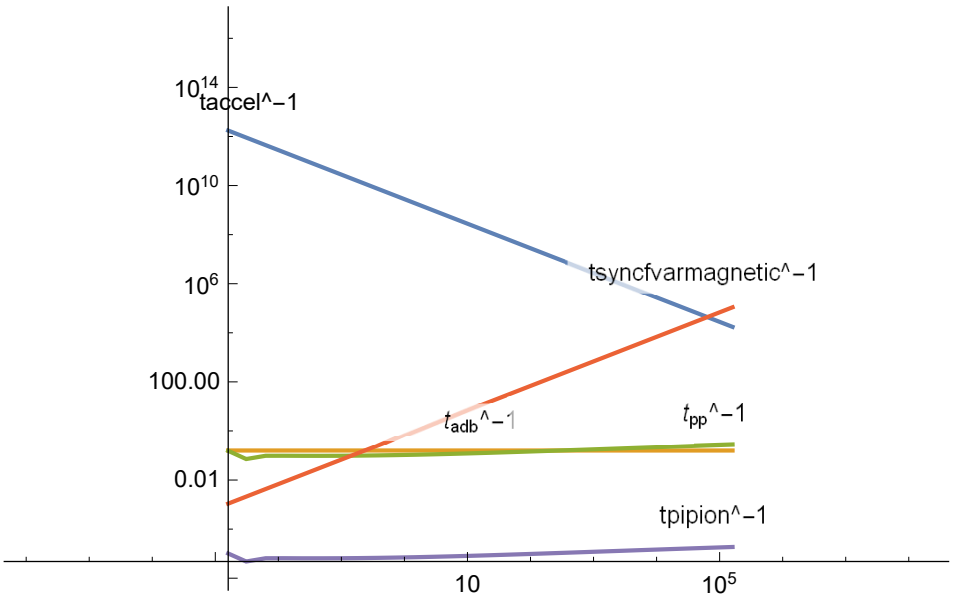

Figure 1: High energy proton distribution loss time scales, for various processes in the jets

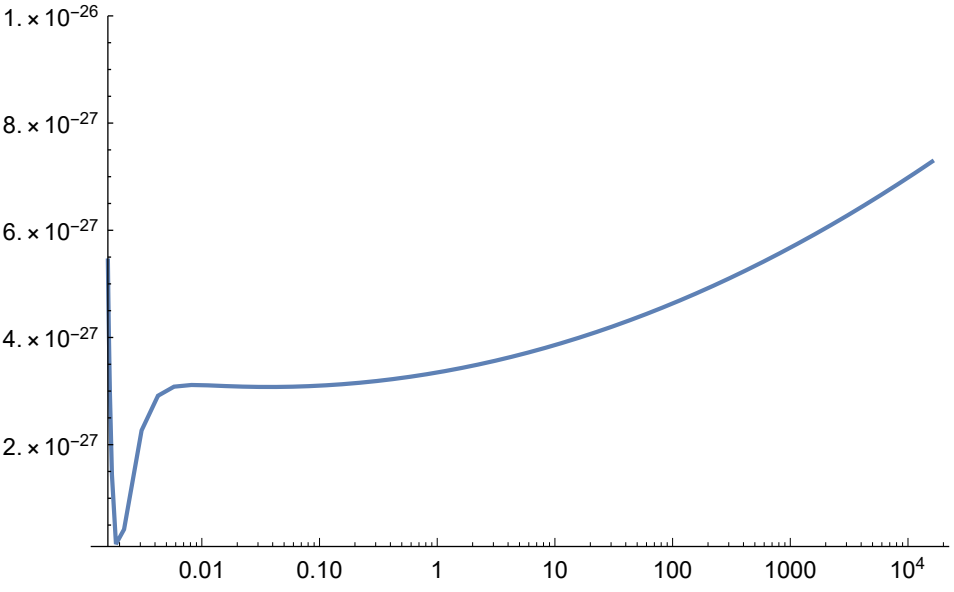

Figure 2: Inelastic proton-proton collission standard plotted with energy.

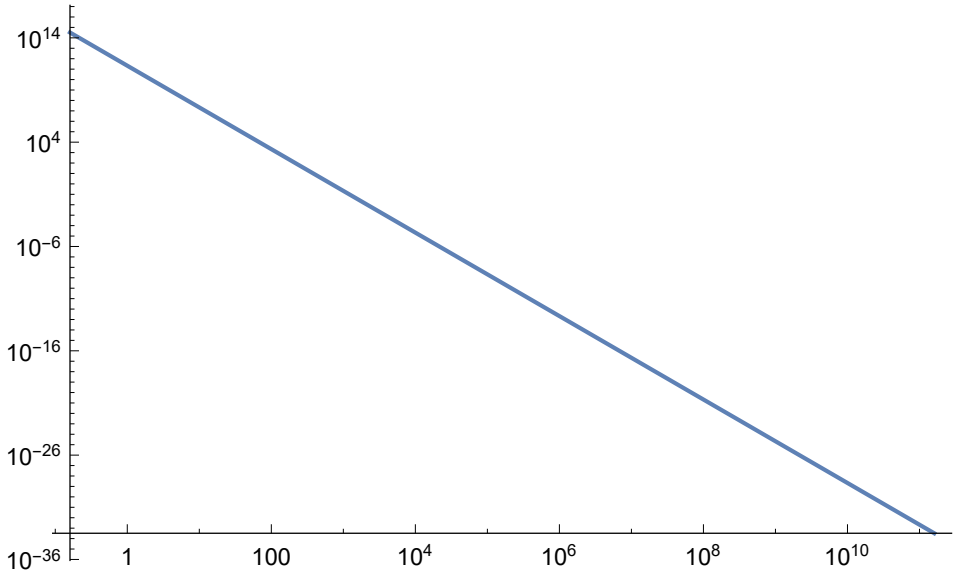

Figure 3: The density of non-thermal protons in the jet is plotted from 100GEV till 1000000000000000 GEV. SOS comment E cutoff SOS

For the adiabatic expansion time scale we have (Reynoso2009)

$$t_{adb} = \frac{1}{\frac{2}{3}\frac{u_{b(adb)}}{z_j}} \tag{3}$$

where z_j=10^{11} cm is the characteristic size scale of the jet to the sides of it. Also, $u_{b(adb)}$ is preset to 0.8, as a representative value throughtout the simulations. For the pion decay time we have

$$t_{\pi 0} = 2.610^{-8} s \tag{4}$$

and

$$t_{\pi} = t_{\pi 0}\Gamma_{\pi} + t_{esc} \tag{5}$$

which in practice is used in nemiss in the form

$$t_{\pi} = t_{\pi 0}(\frac{E_{\pi}}{m_{\pi}c^2}) + t_{esc} \tag{6}$$

where the important parameter of escape time strongly affects the result SOS VERIFY THIS

$$t_{\pi} = t_{\pi 0}\Gamma_{\pi} + t_{esc} \tag{7}$$

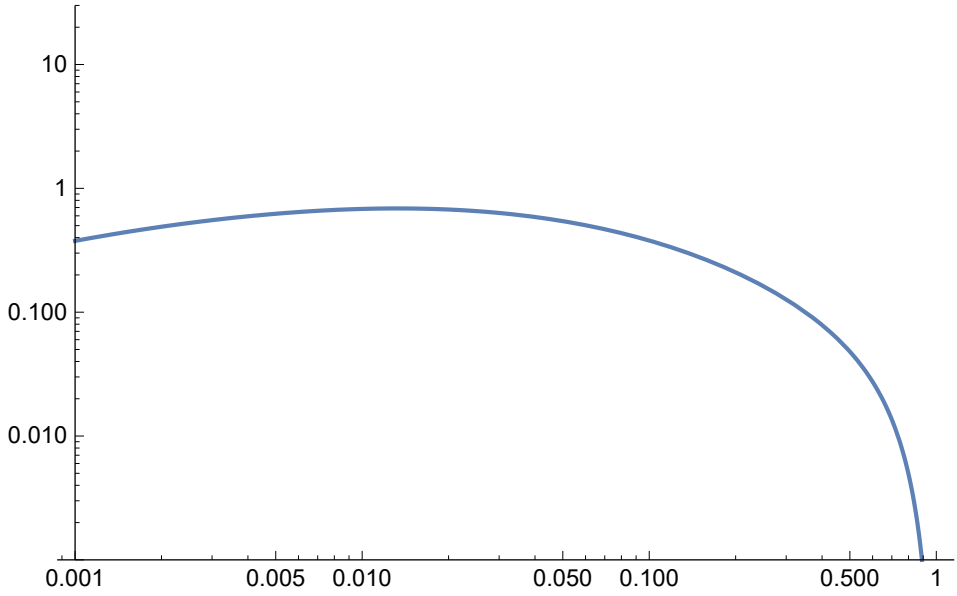

Figure 4: The F function, corresponding to the pion spectrum emerging from a single (hot-cold) proton collision, is presented here, multiplied by the x=$\frac{E_\pi}{E_p}$ fraction SOS verify x. This specific calculation is at E_p=1000 GeV.

The synchrotron loss time scale is defined by

$$t_{sync}^{-1} = \frac{4}{3}(\frac{m_e}{m_p})^3 \frac{1}{8\pi c m_e} \sigma_T B^2 \frac{E_p}{m_p c^2} \tag{8}$$

The form of the latter term, which is essentially Γ_p, facilitates energy-dependent calculations later-on. SOS HERE PUT ZE FIG FROM nemiss SOS verify all ze eqns are above! no one is missing! SOS

3.2. A model for the interaction of thermal and non-thermal protons in the jet.

Hot-cold proton interaction results to a distribution of high energy pions, which then decay allowing the creation of energetic neutrinos. We have (KS17, SK16... pick suitable and ref)

$$pp \rightarrow pp\pi^0 + F_0\,, \tag{9}$$

for charge-free pions (π^0), and

$$pp \rightarrow pn\pi^+ + F_1\,, \qquad pp \rightarrow pn\pi^- + F_2\,, \tag{10}$$

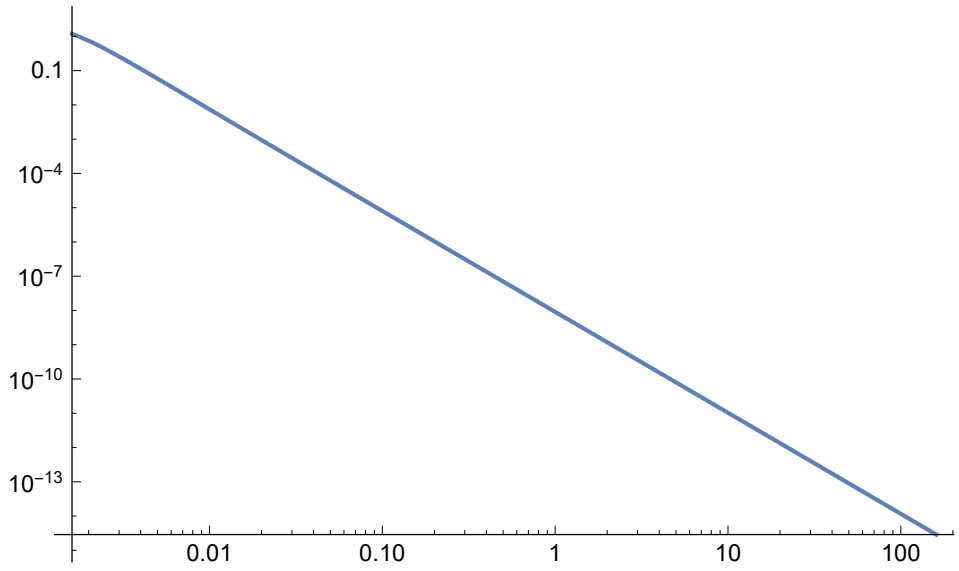

Figure 5: The function Q, describing the combined spectrum from a multitude of (hot-cold) p-p collisions, spanning a range from 1GEV to 100000 GeV.

for charged pions ($\pi^{\pm}$), where F_0, F_1, F_2, represent π^0 and $\pi^+\pi^-$ respectively.

Neutral pions π^0 decay releasing energetic gamma-rays. On the other hand, charged pions π^+ (π^-) decay to muons and neutrinos.

3.2.1. Prompt neutrinos

π^+ or π^- pions weakly decay mostly to an anti-muon or muon and a muonic neutrino or anti-neutrino (ref KS18

$$\pi^+ \to \mu^+ + \nu_\mu \,, \qquad \pi^- \to \mu^- + \widetilde{\nu}_\mu \,. \tag{11}$$

As an approximation, we neglect neutrino production through secondary channels. Furthermore, the processes leading to the production of delayed neutrinos

$$\mu^+ \to e^+ + \nu_e + \widetilde{\nu}_\mu \,, \qquad \mu^- \to e^- + \widetilde{\nu}_e + \nu_\mu \,. \tag{12}$$

are also omitted.

For each particle population in the above cascades, the trasport equation (ref book from 70's for e.g. of nuclear physics, titled trasport theory) is solved

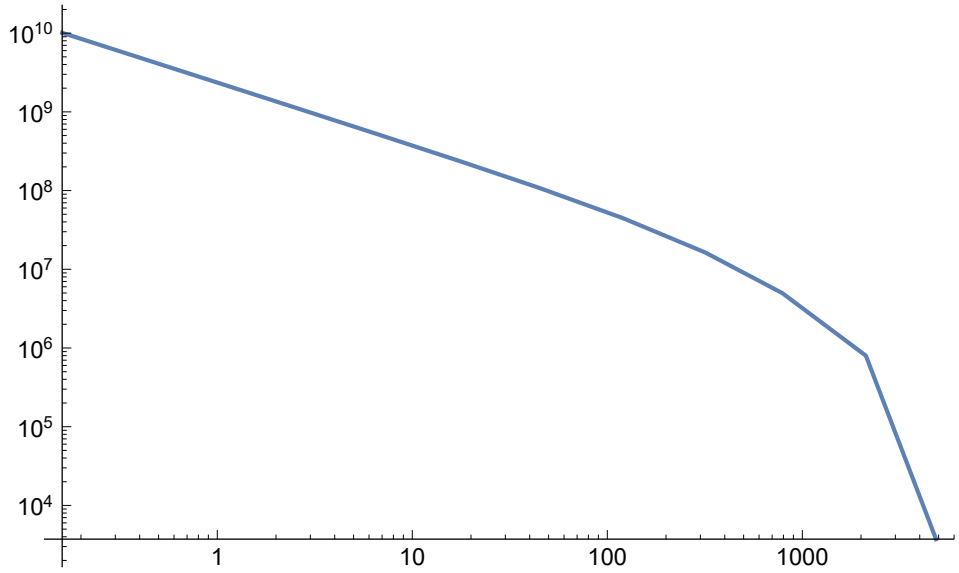

Figure 6: Pion energy distribution, for the range from 100 GeV to 1000000 GeV, plotted in non-normalized units.

successively, SOS HERE PROVIDE ZE EQN, based on eqn 16 later on this paper (ARGS 08,09, book from nuclear 70's, etc russians from 60's ref), . From protons to pions then to muons and neutrinos, each generation of particles becomes the input for the next one. [**?**] calculate the properties of resulting particle distributions over a large energy range, doing fits with Monte Carlo calculations on the QCD results from particle physics.

$$t_{\pi} = t_{\pi 0}\Gamma_{\pi} + t_{esc} \tag{13}$$

In previous works [**? ? ?**], the hadronic jet was modelled using the PLUTO code. The results of PLUTO were then processed in order to calculate the emissivity of γ-rays and neutrino using various approximations. The bulk flow protons spatial density n_z, is obtained from numerical simulation 3D results. In this paper, the neutrino emmisivity is calculated separately at each spatial computational cell, using the angle (los,u), formed between the LOS and the local velocity.

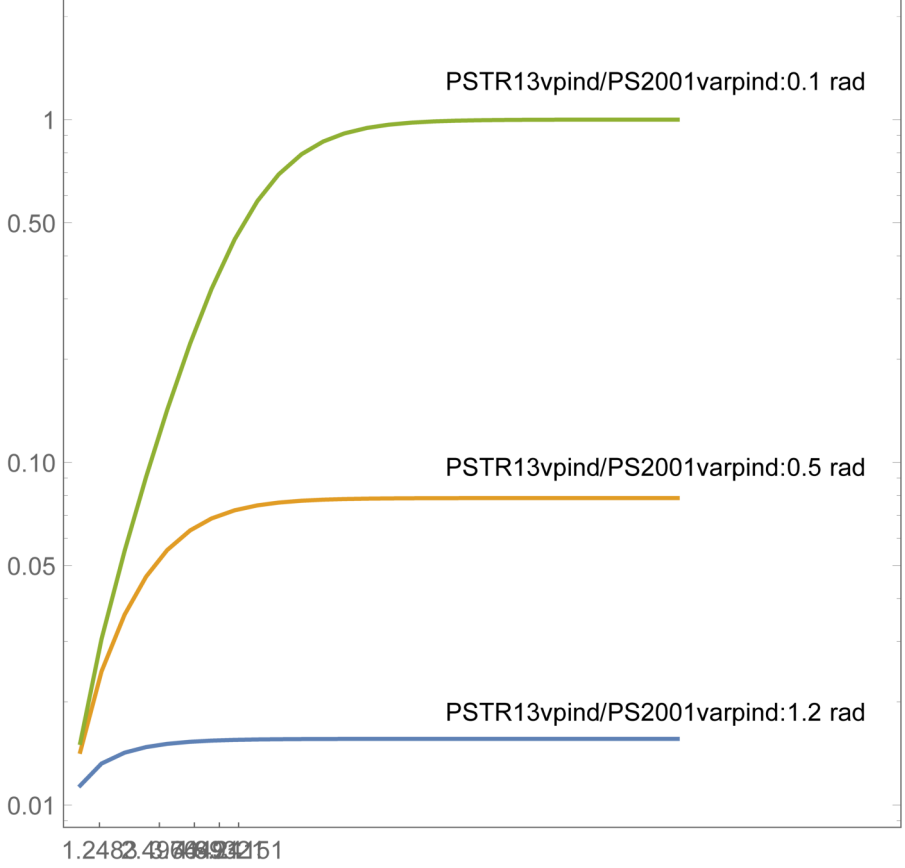

Figure 7: tr13 multi fig starter. XPLAIN

3.3. PS2001 TR11

Furthermore, for the calculation of neutrino emission, the relevant directional equation is: SOS HERE [14], [15], simplified, and also SOS GIVE HERE READY-made multifigure from nemiss! SOS HERE LIES THE SPOT! DO IT HERE! TR13,PS01, multi fig and also equation of TR13 and PS01 SOS

$$t_{\pi} = t_{\pi 0}\Gamma_{\pi} + t_{esc} \tag{14}$$

$$t_{\pi} = t_{\pi 0}\Gamma_{\pi} + t_{esc} \tag{15}$$

$$t_{\pi} = t_{\pi 0}\Gamma_{\pi} + t_{esc} \tag{16}$$

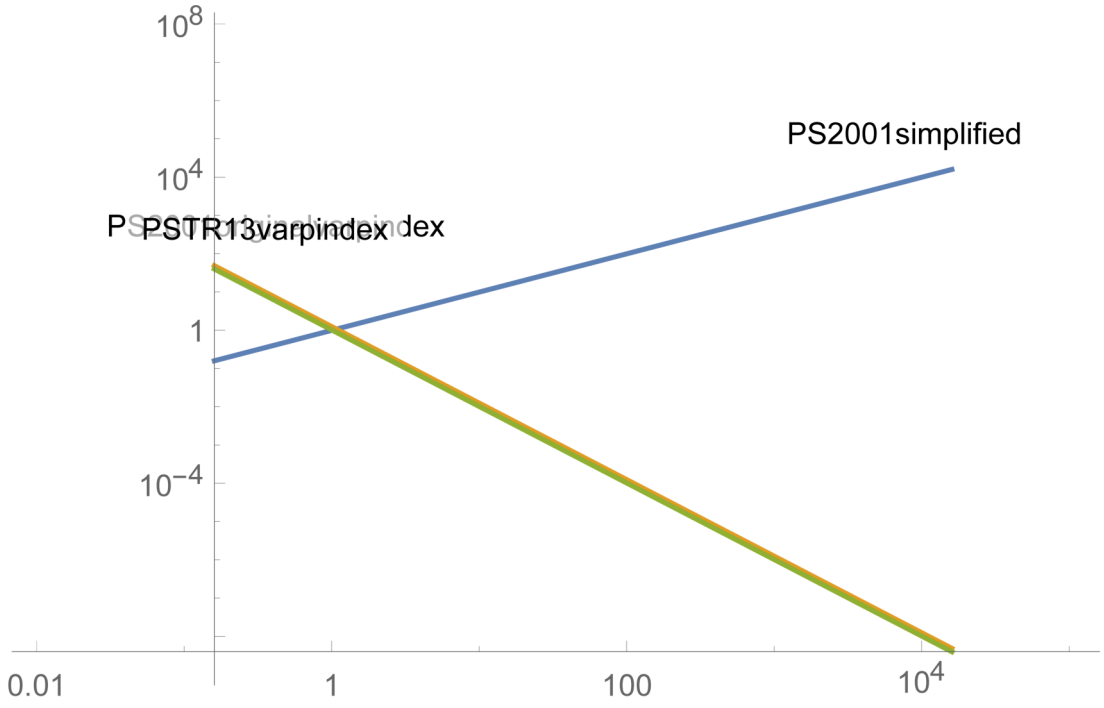

Figure 8: tr13 multi fig base. XPLAIN

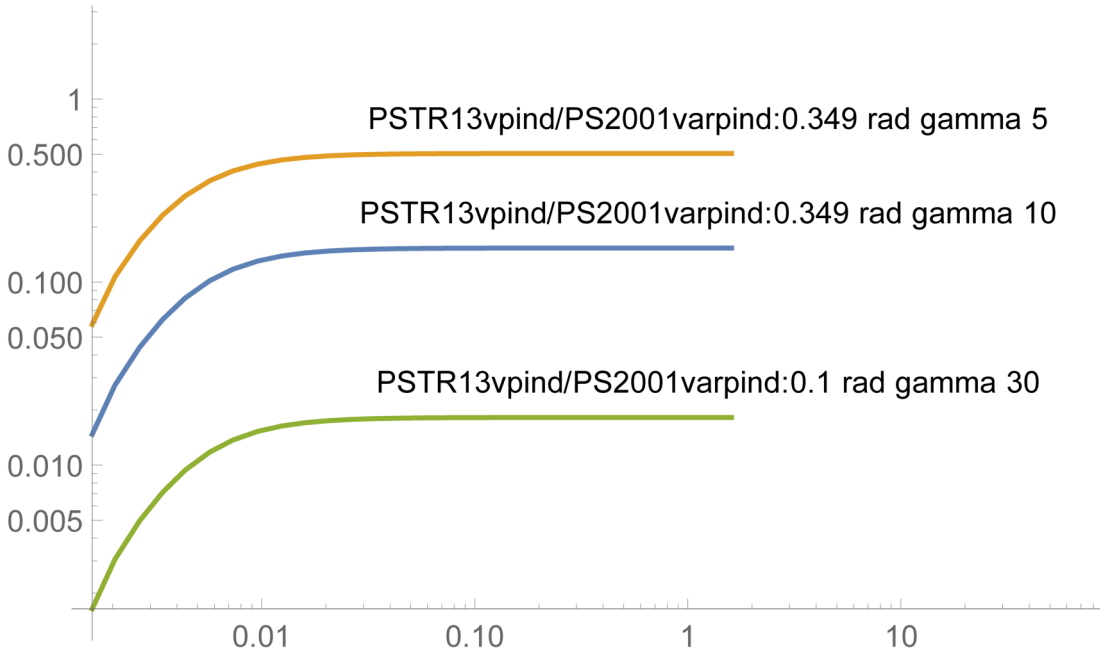

Figure 9: tr13 multi fig third one. XPLAIN

3.4. Pion injection function and pion energy distribution

For each fast-slow proton interaction a spectrum of possible pion energies exists, given by the function F_π ([**?**],[5] and [6]).

$$F_\pi^{(pp)}\left(x,\frac{E}{x}\right) = 4\alpha B_\pi x^{\alpha-1}\left(\frac{1-x^\alpha}{1+rx^\alpha(1-x^\alpha)}\right)^4 \left(\frac{1}{1-x^\alpha}+\frac{r(1-2x^\alpha)}{1+rx^\alpha(1-x^\alpha)}\right)\left(1-\frac{m_\pi c^2}{xE_p}\right)^{\frac{1}{2}} \quad (17)$$

where $x = E/E_p$, $B_\pi = a' + 0.25$, $a' = 3.67 + 0.83L + 0.075L^2$, $r = 2.6/\sqrt{a'}$, $\alpha = 0.98/\sqrt{a'}$,

and L is SOS GIVE L HERE FROM Kelner06, ARGS09 and also from code (IT IS NOT JET LUMINOCITY, as haris and his offspring have written!) (see [5**?**]).

SOS MAYBE WE PLOT THIS MAYBE NOT CHECK IT OUT! SOS run nemiss alone, no need to upgrade VM, just run nemiss alone, not pload5D!.

In Fig. xF_π is plotted with the fraction x, for three different hot proton energies (E_p=10^3GeV, E_p=10^4GeV, E_p=10^5GeV)

The pion injection function, $Q_\pi^{(pp)}$, comprises, at each pion energy, the weighted pion contributions, to that pion energy, from the spectrum F, of all possible p-p interactions.

$$Q_\pi^{(pp)}(E,z) = n(z)c\int_j^1 \frac{dx}{x}\left(\frac{E}{x},z\right)F_\pi^{(pp)}\left(x,\frac{E}{x}\right)\sigma_{pp}^{(inel)}\left(\frac{E}{x}\right), \quad (18)$$

SOS j, not k! $j = E/E_p^{(max)}$. x is the fraction of the pion energy to proton energy, σ_{pp}^{inel} is the inelastic p-p scattering cross section, and $n(z)$ is the bulk flow proton density.

SOS DO OUR OWN PLOT of Qpi, from nemiss easy-peasy from mathem! In Fig. 2 (right panel), we plot the $Q_\pi^{(pp)}$ versus the pion energy E_π for three different jet densities (n=10^9, n=10^{10}, n=10^{11}). We notice the approximate

square dependence of the scale of $Q_\pi^{(pp)}$ on the jet density, which is because N_p also depends on $n(z)$.

SOS HERE SAY IT CORRECLTY, UNLIKE THEM!!! REMEMBER TRANSPORT EQUATION HOW IT WORKS, AKA CHEMICAL BALANCE EQUATION: TWO POPULations, mother and daughter, exchanging members according to a reaction!!! SAY IT NICELY !!! maybe also move this earlier on, 221120 SOS

SOS 300420 RUSSIANS SAY ABOUT ANISOTROPY OF HOT PROTON DISTRO BEING REFLECTED, for neutrinos, to neutrino distro in jet system then projected off axis REINFORCED for lab frame!! SOS LOOK INTO ISOTROPY of hot proton distro in jet frams, its origins, shcks, per cell, etc shocks vs single cells, etc!!

SOS LOSS TIMES HERE Ref from earlier sos say each thingy just once! loss times ref here to earlier appearance!

In order to obtain the pion distribution, we solve the SOS MERGE WITH EARLIER TR. EQN stuff SOS following transport equation

$$\frac{\partial N_\pi}{\partial E} + \frac{N_\pi}{t_{loss}} = Q_\pi^{(pp)}(E,z) \tag{19}$$

where $N_\pi(E,z)$ denotes the pion energy distribution. We proceed

$$N_\pi(E) = \frac{1}{|b_\pi(E)|} \int_E^{E^{(max)}} dE' Q_\pi^{(pp)}(E') \exp\left[-\tau_\pi(E,E')\right], \tag{20}$$

where

$$\tau_\pi(E',E) = \int_{E'}^{E} \frac{dE'' t_\pi^{-1}(E)}{|b_\pi(E'')|}. \tag{21}$$

The above are performed for each computational cell, where quantities, for radiative purposes, are considered locally constant, making particle population transport dependent on energy. SOS HERE VS RUSSINS FOR SCATTER VS IRRADIANCE ETCWe also take the characteristic scale (mean free path) of the radiative interactions to be smaller than the cell size, leading to the containment

of particle interactions within a given hydrocode cell. Furthermore, the time scale for the radiative interactions is so much smaller than the hydrocode's timestep, that the radiative interactions belong to a single timestep each time.

A cell is macroscopically large, inasmuch only the deterministic portion of the transport equation is employed, rendering it deterministic.

3.5. Neutrino emissivity

The emissivity of prompt neutrinos [**? ? ? ?**], is

$$Q_{\pi\to\nu}(E) = \int_{E}^{E_{max}} dE_\pi t_\pi^{-1}(E_\pi) N_\pi(E_\pi) \frac{\Theta(1-r_\pi-x)}{E_\pi(1-r_\pi)}\,, \tag{22}$$

$x = E/E_\pi$ and t_π is the pion decay timescale. $\Theta(\chi)$ is the theta function [5, 16].

The neutrino emissivity (sos fluence vs emissivity, solid angle, etc LU blue book's chapters on such things, we got its photocopies dig 'em up! else, wiki or something! on) is calced for each individual cell, using the cell's own angle to the cell's LOS to the observer (included is PS01/TR13). The imaging process may either incorporate parallel LOs's or a focused beam, where each LOS follows a slightly different path to a common focal poiont. focal point selection is based on the magnification, i.e. resoluion of the detection process. For this paper, we select TABLE OF RUNS HERE! ....SOS ALSO DO INCLUDE the ability of a varianle alpha spectral index in nemiss! imaging geom selection describe here SOS. A synthetic image of the model system is thus produced. The hydrocode run is fully included in the calc. SOS here speak about hot proton isotropy, or anisotropy, based on derishev 06 etc. SOS DO IT. ALSO DO it for many different energies.

here give runs methodology. SOS one case use, not many! next paper the rest! Briefly describe nemiss and rlos here. RLOS in appendix SOS save stuff for next paper SOS. ALSO use a varialbe alpha spectral index, aka ARGS19. SOS do one now, the rest in next paper!

4. Results and discussion

4.1. Model setup

RUN a pluto sim. twin jet SOS. THEN for many angles to the los. (but cyg x-1 is known angle! use uncertainty!! do different angles! for each angle, do a whole jet run and add up emission. normalize 'em. Repeat for 7-8 energies. RUN it in multiple spawns, in multiple dirs. have the dirs prepped from beforehand. thus pseudo-paralel. In total, SED spectrum for each angle. DO IT FIRST FOR PIONS, if all ok then for neutrinos. PIONS precursosr, much faster!. SOS do it also for HJ88 jet, compare to HOLLANDIANS 2020 grb, no z redshift. ALSO DIG UP MQ off axis. compare off axis cells pointing, hot proton anisotropy and D off axis scaling. ALSO USE granot2012 scaling to ease up a bit on the calcs, where possible! PRINT those scaling papers!)

SOS UPDATE HERE DESCRIPTION OF twin jet sim, med res, on which to do the above!

The jet base is situated near the centre of a Cartesian XYZ grid.

An intermittent model jet, representing a microquasar system, injected at u_{jet} =0.865c is studied with the RMHD setup of the PLUTO hydrocode, at a uniform grid resolution of 60 $\times$ 100 $\times$ 50 SOS also we may do one HR SOS maybe. In all of the model runs the same initial jet density of 10^{10} protons/cm^3 is used, 10 times less than the maximum surrounding gas density. Winds comprise an accretion disk wind construct and a stellar wind, which falls off away from the companion star, located off-grid at (400, 0, 400 SOS THIS HAS CHANGED NOW, due to twin jet setup SOS check it! SOS), while the jet is threaded by a strong confining toroidal magnetic field of B=400 simulation units. Blobs are emitted during the first 1.5 out of every 10 time units (simulation seconds), for both the u=0.26c and the u=0.8c models, while for the u=0.6c case, the jet is on during the first 5 out of every 50 time units. The simulations were run until at least t = 750, saving a data snapshot every 15 time units. Taken from the u=0.6c model run, a snapshot of density is shown in Figure 10, in both 2D and 3D, where we can see the magnetically collimated

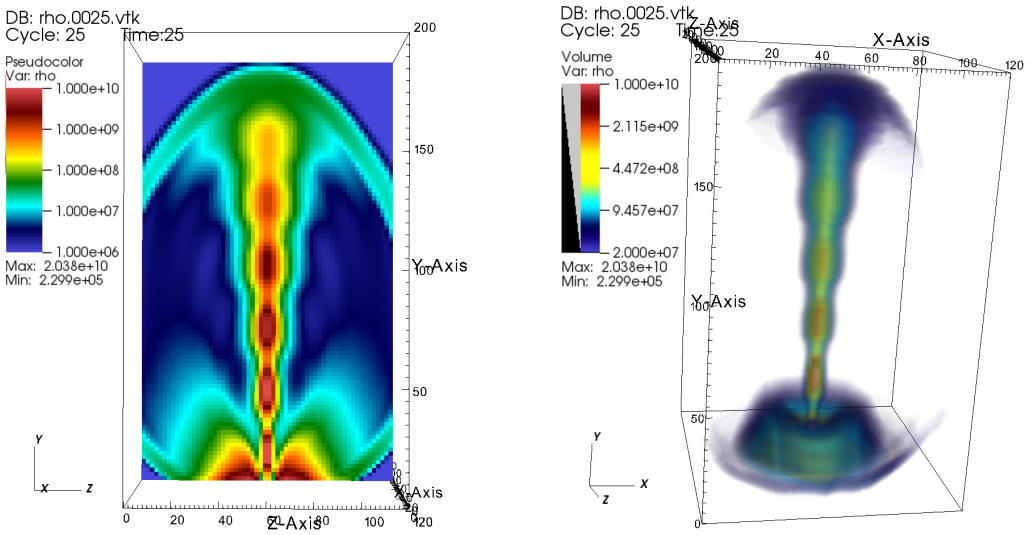

Figure 10: SOS REPLACE WITH A PLOT FROM OUR SIMS! ALSO WITH ONE OTHER FROM THE HIGH RESOLUTION ONE, as a demo!! SOS DO EM! Snapshot 25 of the u=0.6c hydrocode run, corresponding to a model time of t=375 (25 × 15), depicting the density. We can see the jet front reaching the end of the grid, having advanced though increasingly lighter surrounding winds, after crossing the simplified accretion disk wind construct. On the left is presented a slice cut throught the data and on the right a 3-dimensional density plot. Image produced with VisIt.

sequence of plasmoids advancing through surrounding winds.

SOS PLOT FROM PLUTO. 2D/3D, esp HR if possible! PLUTO HR and MR are the SAME, nemiss output is different per case!

NEMISS RUNS HERE BRIEFLY DESCRIBE ZE PARAMS SOS

RLOS was then run, based on the above hydrocode data, with sfactor=1 for the pload shrink factor. In general, the imaging process may or may not use all snapshots available to it, depending on the light crossing time of its model segment (potentially adjusted through the clight parameter). Trying to read more snapshots than loaded corrupts the hydrocode time array, called T, resulting to errors. NEMISS HERE RUNS DESCRIBE runs aka results ! SOS! plots here of both lines and also synthetic images! also a high res image perhaps? also, do mention variaibility on a per cell basis!

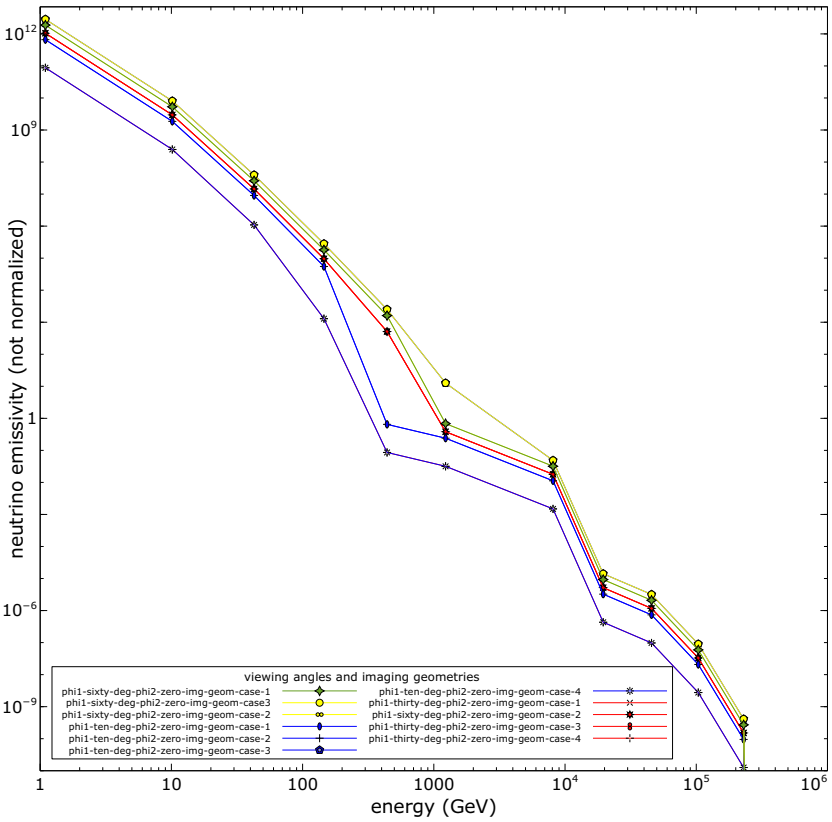

Figure 11: non-normalized SED from a series of sims, see array for details! SOS ADD SOME here

5. Conclusions

SOS HERE PLACE DISCUSSION AND CONCLUSIONS

References

[1] I. F. Mirabel, L. F. Rodríguez, Ann. Rev. Astron. Astrophys37 (1999) 409.

[2] G. E. Romero, D. F. Torres, M. M. Kaufman Bernadó, I. F. Mirabel, Hadronic gamma-ray emission from windy microquasars, Astron. & Astrophys.410 (2003) L1–L4. arXiv:astro-ph/0309123, doi:10.1051/0004-6361:20031314-1.

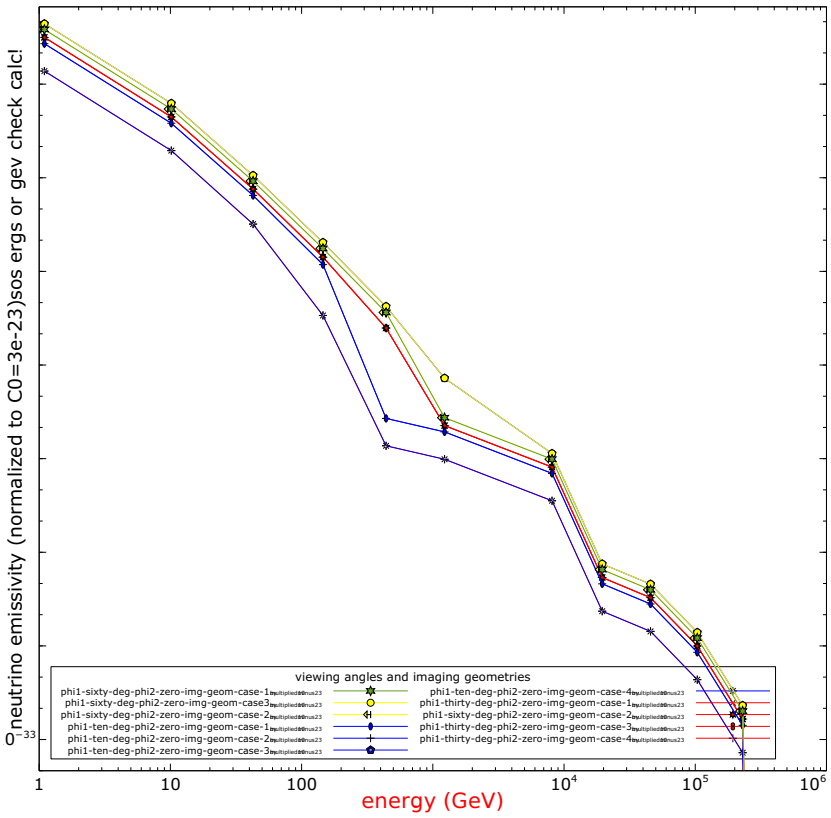

Figure 12: Normalized SED from a series of sims, see array for details! SOS ADD SOME here

[3] W. Bednarek, TeV Neutrinos from Microquasars in Compact Massive Binaries, Ap. J.631 (1) (2005) 466–470. arXiv:astro-ph/0505547, doi:10.1086/432411.

[4] M. M. Reynoso, G. E. Romero, H. R. Christiansen, Production of gamma rays and neutrinos in the dark jets of the microquasar SS433, MNRAS387 (4) (2008) 1745–1754. arXiv:0801.2903, doi:10.1111/j.1365-2966.2008.13364.x.

[5] M. M. Reynoso, G. E. Romero, Magnetic field effects on neutrino production in microquasars, Astron. & Astrophys.493 (1) (2009) 1–11. arXiv:0811.1383, doi:10.1051/0004-6361:200811004.

[6] M. M. Reynoso, A. M. Carulli, On the possibilities of high-energy neu-

trino production in the jets of microquasar SS433 in light of new observational data, Astroparticle Physics 109 (2019) 25–32. arXiv:1902.03861, doi:10.1016/j.astropartphys.2019.02.003.

[7] D. Koessl, E. Mueller, W. Hillebrandt, Numerical simulations of axially symmetric magnetized jets. I - The influence of equipartition magnetic fields. II - Apparent field structure and theoretical radio maps. III - Collimation of underexpanded jets by magnetic fields, Astron. & Astrophys.229 (2) (1990) 378–415.

[8] F. M. Rieger, P. Duffy, A Microscopic Analysis of Shear Acceleration, Ap. J.652 (2) (2006) 1044–1049. arXiv:astro-ph/0610187, doi:10.1086/508056.

[9] F. M. Rieger, An Introduction to Particle Acceleration in Shearing Flows, Galaxies 7 (3) (2019) 78. arXiv:1909.07237, doi:10.3390/galaxies7030078.

[10] Singh2019MHD, Study of relativistic magnetized outflows with relativistic equation of state, Monthly Notices of the Royal Astronomical Society 488 (4) (2019) 5713–5727. arXiv:https://academic.oup.com/mnras/article-pdf/488/4/5713/29191239/stz2101.pdf, doi:10.1093/mnras/stz2101.
URL https://doi.org/10.1093/mnras/stz2101

[11] t. . T. j. . . k. . A. y. . . m. . j. v. . . p. . . a. . a. e. . a. p. . a. a. . h. a. . P. Fabrika, S.

[12] M. C. Begelman, R. D. Blandford, M. J. Rees, Massive black hole binaries in active galactic nuclei, Nature287 (5780) (1980) 307–309. doi:10.1038/287307a0.

[13] E. V. Derishev, F. A. Aharonian, V. V. Kocharovsky, High-energy emission from off-axis relativistic jets, in: F. A. Aharonian, H. J. Völk, D. Horns (Eds.), High Energy Gamma-Ray Astronomy, Vol. 745 of

American Institute of Physics Conference Series, 2005, pp. 510–515. arXiv:astro-ph/0501197, doi:10.1063/1.1878454.

[14] D. F. Torres, A. Reimer, Hadronic beam models for quasars and microquasars, Astron. & Astrophys.528 (2011) L2. arXiv:1102.0851, doi:10.1051/0004-6361/201116488.

[15] D. Purmohammad, J. Samimi, On the hadronic beam model of TeV gamma-ray flares from blazars, Astron. & Astrophys.371 (2001) 61–67. doi:10.1051/0004-6361:20010308.

[16] T. Smponias, O. Kosmas, Advances in High Energy Physics 921757.

[17] D. Weiskopf, Dissertation, Ph.D. thesis, Dissertation, der Eberhard-Karls-Universitat zu Tubingen, der Fakultat fur Physik (2001).

[18] T. V. Cawthorne, in: Hughes (Ed.), Beams and Jets in Astrophysics, Cambridge University Press, 1991.

[19] P. A. Hughes, in: Hughes (Ed.), Beams and Jets in Astrophysics, Cambridge University Press, 1991.

[20] W. B. Sparks, D. Fraix-Burnet, F. Macchetto, F. N. Owen, A counterjet in the elliptical galaxy m87, Nature 355 (1992) 804.

[21] R. Laing, A. H. Bridle, Relativistic models and the jet velocity field in the radio galaxy 3c 31, Monthly Notices of the Royal Astronomical Society 336 (2002) 328.

[22] T. Smponias, T. S. Kosmas, MNRAS412 (2011) 1320.

[23] T. Smponias, T. S. Kosmas, MNRAS438 (2014) 1014.

[24] O. Kosmas, T. Smponias, aHEP accepted (2018).

[25] R. M. Hjellming, K. J. Johnston, ApJ 328 (1988) 600.

[26] A. Mignone, G. Bodo, S. Massaglia, T. Matsakos, O. Tesileanu, C. Zanni, A. Ferrari, Ap. J. Supp.170 (2007) 228.

6. Appendix

070321 SOS here we put normalization calc tetradio

6.1. Normalization

In this section, we shall perform the normalization of the arbitrary units plot to the scaled simulated emission from the model jet.

The kinetic energy of the jet at its base can be expressed as

$$E_k = \frac{1}{2}(\Gamma m)u^2 \tag{23}$$

where u is the jet speed, and m the mass of a jet portion crossing the cross section of the jet there. Then, the jet kinetic power, is the kinetic energy traversing the cross section per unit time

$$P_k = dE_k/dt = \frac{1}{2}(\Gamma dm/dt)u^2 \tag{24}$$

where the speed is taken constant during an ejection episode (it is also set constant in the simulation described here). But

$$dm/dt = \rho dV/dt = \rho A dx/dt = \rho A u \tag{25}$$

where A is the jet base cross section area, also taken constant both in the simulation and here. Therefore

$$P_k = dE_k/dt = \frac{1}{2}(\Gamma \rho A)u^3 \tag{26}$$

or

$$P_k = dE_k/dt = \frac{1}{2}(\Gamma \rho N_{cell} L_{cell}^2)u^3 \tag{27}$$

where $A = N_{cell}L_{cell}^2$. L_{cell}^2 is the area of the side of length L_{cell} of a cubical computational cell, at the jet base, and N_{cell} is the number of such cells forming the jet base. We then express density as a function of proton number density N_p and proton mass m_p

$$\rho = N_p m_p. \tag{28}$$

Furthermore, we introduce a factor $\alpha = L_\nu/L_k$, representing the portion of jet power emitted in neutrinos. A typical value is taken as 10^{-3}. We also set $\beta = uc$. Also, we take into consideration a less than unity, positive filtering factor f_f, which accounts for not using all of the jet cells, but only those with velocity orientation closer to the LOS and also with speed above a given limit. So far, we then have

$$L_\nu = \alpha L_k = \alpha P_k = \alpha dE_k/dt = f_f \frac{1}{2}\alpha(\Gamma(N_p m_p)N_{cell}L_{cell}^2)\beta^3 c^3 \tag{29}$$

The intensity of the jet is then expressed as $I_\nu = L_\nu/4\pi D^2$, where D is the distance to Earth. Thus

$$I_\nu = f_f \frac{1}{4}\pi D^2 \alpha \frac{1}{2}(\Gamma(N_p m_p)N_{cell}L_{cell}^2)\beta^3 c^3 \tag{30}$$

our simulation, the jet beam travels at $\beta=\frac{u}{c}$ =0.866, with a density of 10^{10} protons/cm^3. L_{cell} is 10^{10} cm, while the number of cells comprising the beam, at its base, at this resolution, is $N_{cell} \simeq 15$. Γ is also calced using β. The distance to Earth, is taken here with a typical value of D=5 kpc, or approximately 10^{25} cm.

We then integrate the area under the curve of the arbitrary units plot, for the case of (which case of data was it? SOS it matters!). We do a cumulative sum over the roughly ten points, admitting a ten percent linear portion per order of magnitude scale level. Thus, we find 9.85*10^{1}0, which means that our sum is ten times smaller, or approximately 10^{1}0, in arbitrary units (AU)*GeV. We replace an AU with a constant C_0, so that AU= C_0 erg/(s*cm^2) MAYBE per GeV here as well SOS!. Then the plot area equals integral of Inu =DE (PLOT AREA)*C_0 erg/(s cm^2) GeV. This we also set equal to the intensity of the neutrino portion of the kinetic luminocity, arriving at Earth, $L_\nu/(4\ \pi\ D^2)$. Therefore

$$I_\nu = f_f \frac{1}{4}\pi D^2 \alpha L_k \tag{31}$$

or

$$I_\nu = f_f \frac{1}{4}\pi D^2 \alpha \frac{1}{2}(\Gamma(N_p m_p)N_{cell}L_{cell}^2)\beta^3 c^3 \tag{32}$$

we set the above equal to the area under the plot, expressed in units of C_0, in order to find the latter (normalization constant)

$$I_\nu = f_f \frac{1}{4}\pi D^2 \alpha \frac{1}{2}(\Gamma(N_p m_p) N_{cell} L_{cell}^2)\beta^3 c^3 = (PLOTAREA) * C_0 erg/(scm^2) GeV \tag{33}$$

Fo our case, we find $C_0 = 3^* 10^{-23}$ SOS units, which is the value of the arbitrary unit C_0. Thus the intensity is as in plot (ref normalized plot here. Only C0 in main text!) re do ze calcs in the margin of the preprint one last time perhaps! verify!

Using the above constant, we multiply by it the value given in arbitrary units for the particle emission. We then arrive to the updated plot (....) which may be directly compared to other models and to observations. MAIN TEXT THE REST of the sample application!

6.2. Relativistic Effects

The main effects of the Lorentz/Poincaré transform on the emission from a relativistic object [17], specifically applied to an astrophysical jet, are relativistic aberration, time dilation and frequency shift [18, 19, 20, 21].

6.2.1. Lorentz factor

The Lorentz factor for a hydrocode cell is [19]

$$\Gamma_{Lorentz} = \frac{1}{\sqrt{1-u^2}} \tag{34}$$

where

$$u = \sqrt{u_x^2 + u_y^2 + u_z^2} \leq 1 \tag{35}$$

is the value of the local velocity $\vec{u} = (u_x, u_y, u_z)$, in units of the speed of light.

191120 SOS THIS ONE SECTION NOT FOR NEUTRINOS, gamma rays ONLY!

201120 SOS apo edo typed SOS

SOS! 201120 SOS can bow do both here! say Dfactor and then link to PS01/TR13 similar boosting SOS

6.2.2. Doppler factor calculation

Jet radiation is either boosted or de-boosted, depending on the angle losu, between the direction of the LOS and $\vec{u}$. The higher the jet speed, the narrower and stronger the cell boost cones around the jet head direction. On the other hand, outside cell boost cones, *de*-boosting occurs, that is to say the higher the velocity is, the weaker the signal becomes. D equals

$$D = \frac{\sqrt{1-u^2}}{(1 - u * cos(losu))} \tag{36}$$

here REF to eqn of PS01/TR13 given above SOS

For both the above equations, the angle between the LOS and the local velocity vector is required at every point of the computational space.

The cosine of angle losu is calculated in the following manner:

Let us define a fiducial unitary LOS vector $(\vec{LOS}) = (lx_1, lx_2, lx_3)$, with $(LOS) = \sqrt{lx_1^2 + lx_2^2 + lx_3^2} = 1$. In the following, ϕ_1 and ϕ_2 represent azimuth and elevation angles 1 and 2, respectively.

$$lx_1 = cos(\phi_1)cos(\phi_2),\ lx_2 = sin(\phi_1)cos(\phi_2),\ lx_3 = sin(\phi_2) \tag{37}$$

$$\vec{LOS} * \vec{u} = (LOS) * u * cos(\widehat{\vec{LOS}, \vec{u}}) = \vec{LOS} * \vec{u} = lx_1 * u_x + lx_2 * u_y + lx_3 * u_z \tag{38}$$

Therefore, we have ((LOS)=1)

$$cos(\widehat{\vec{LOS}, \vec{u}}) = \frac{lx_1 * u_x + lx_2 * u_y + lx_3 * u_z}{(LOS) * u} = cos(\widehat{\vec{LOS}, \vec{u}}) = \frac{lx_1 * u_x + lx_2 * u_y + lx_3 * u_z}{\sqrt{(u_x^2 + u_y^2 + u_z^2)}} \tag{39}$$

A miniscule number is added to the denominator of equation 39, in case u=0. The above calculation allows the assignement of a Doppler boosting factor, through equations 35, 36 and 39, to each discrete emission event along a line of sight.

6.2.3. Doppler boosting

The jet spectrum is given by

$$S_{jet} = SOS - JET - FRAME - SPECTRUM - PUT - HERE \tag{40}$$

Earth frame jet emissivity S_{obs} can be expressed [19, 18] as (SOS REF2 says Sjet is spectrum, Dtothe3plusa is emissivity)

$$S_{obs} = S_{jet} D^{3+\alpha} \tag{41}$$

where α is the spectral index. The exponent $(3+\alpha)$ in the above can be broken down into different contributions from separate effects. Two units come from the aberration of light, one from the relativistic dilation of time and α from the effect of frequency shift, while for a continuous optically thin jet a D factor is lost [18].

Power-law Lorentz transform. SOS HERE TR11/13 STUFF! SOS INSERT FORMULA HERE! PLOT HERE TR13 REPRODUCE AS WELL! SOS PLOT TR13 HERE!!! ALSO PS01 vs simple vs TR13 SOS HERE! TWO PLOTS PUT! SOS THESE NOT NEEDED FOR NEUTRINOS, MAY PROVE USEFUL FOR GAMMA RAYS. IN NEUTRINOS, there is the shift included in the PS2001 expression, or the TR13 one!

Aberration-searchlight effect. Relativistic aberration changes the perceived direction of light (there is no curving in SR (ref 2)), when transforming between the jet frame and the earth frame, 'tilting rays', emanating from the jet, generally towards its head area. A jet element is assumed, for simplicity, to emit isotropically in its own frame of reference SOS HERE

SUPER SOS THIS VS DERISHEV ET AL 2006, anisotropy of jet cell emission, aka hot rpoton distro jet frame isotropy RIEGER ET AL 07,19,marcovith 20 SOS isotropy briefly refer to here! 1st approximation.

Cell emission along a ray *within* the cell's boost cone, is then reinforced accordingly, while if *outside* the cone it is weakened. Depending on the local velocity value and direction, succesive or neighbouring cells may have totally different boost cones.

Time dilation. Time dilation contributes one D factor to the emission result.

SOS 290319 briefly xplain the reasoning behind each test (clight, ts, etc) right where those tests are first presented.

SOS 290319 Add the tests on SR imaging (steadsy-state ones) vs Kraus etc from the lit., . Move all tests to Appendix. only keep APP in main text.

1. sphere. st state. static and moving sphere.

2. rod, as aportion of a cylindrical jet. (should be implemented already)

3. A sphere emitting isotropically, transformed to the obs frame. based on hughes 91

4. A st. state hj88 type jet, transformed to the obs frame. based on cawthorne in hughes 91.

5. A, optically thin SYNCHROTRON st. state hj88 type jet, transformed to the obs frame. also based on cawthorne 91, a bit later on (simple synchr. jet dependent on sin theta dash: S(nu, theta)=Snu(dash)Dtothe(3+a), or 2+a for simple jets (replies to ref2 comment)

Comment: a tangled B field also contributes to the synchrotron emission being isotropic. see if this is the case for thermal or radio as well.

some good refs from cawthorne 91: BBRees84 and RL79 chapter 4. SOS re-examine those SOS.

SOS briefly explain the reasoning behind each test, such as clight, ts, etc.

SOS 020520 DONE IS SUMMER of 19 SOS HERE describe focuing of the beams and add a relevant figure. SOS 040419

compare focused results to the kraus et al results. SOS

move sall tests to the appendix only keep basics in main text.

ROD TEST: kraus et al pre-applies length contraction then runs their sp. relat. ray tracing model. We do not pre-apply length contraction, say that and take into account whemn comparing.

040419 we may improve on the steady state tests by incorporating elements from computer graphics, such as parametric moving object representation. Also, we do not adopt diffraction,e tc, only a straight line of sight. XPLAIN that!

6.3. 3-dimensional imaging

The 3D setup of RLOS emulates that of its ancestor classical imaging code ([22, 23, 24]). From each pixel of the "imaging" side, of the 3D computational

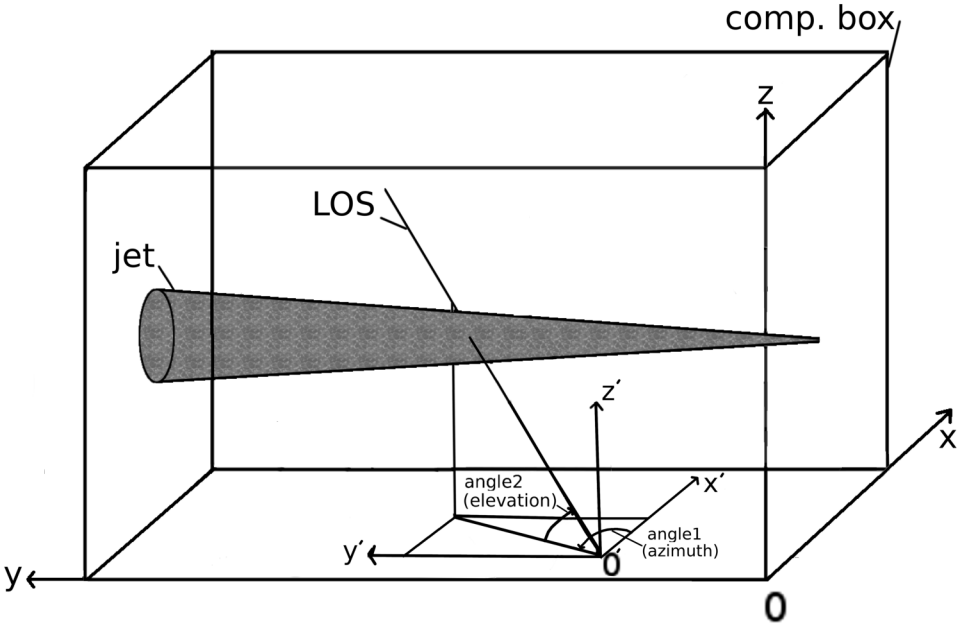

Figure 13: A 3D schematic view, of RLOS applied to a model astrophysical jet. The imaging side of the computational box is the yz plane, located on the side of the box apparently closer to the reader. Lying on the yz plane, O′ is the point of origin of a random LOS, with its own dashed coordinate system x′y′z′. Alternatively, the imaging plane may also lie on the xz side of the box. The final image is taken to formed on the eye or detector of a fiducial observer, situated at the end of the LOS.

domain (Figure 13), a line of sight (LOS) is drawn, through the imaged volume. Along the LOS, the equation of radiative transfer is solved at each cell, using local emission and absorption coefficients. Depending on the situation modelled, coefficients may either be calculated directly, or outsourced to another program.

Lines of sight are drawn, starting from a pixel of the yz-side or xz-side (either way called the imaging side) of the domain, tracing their way along the given direction (Figures 13 and 14), until they reach a length of $\sqrt{(x_{max}^2 + y_{max}^2 + z_{max}^2)}$, where $x_{max}, y_{max}, z_{max}$ are the dimensions, in cells, of the computational domain. In practice, on reaching the ends of the domain a LOS calculation halts, therefore some LOS's end up shorter than others. The above process is repeated within a 2D loop, running over the imaging plane,

each LOS corresponding to a single pixel of the final synthetic image. Along a LOS, no sideways scattering is considered SOS 290319 DIG UP REF for that cos ref2 asked why no scsttering? SOS.

A model astrophysical system may be inserted into RLOS directly, for example forming a 'conical' jet setup [25]. Alternatively, data output from a hydrocode may be employed, which is the case in the current paper, using PLUTO [26].

6.4. Time-resolved imaging

6.4.1. Accessing 4-dimensional data

The finite nature of the speed of light affects the appearance of a fast-moving object in a crucial manner. Consequently, drawing a relativistic image of an astrophysical system, necessitates the availability of information regarding not only its spatial properties, but its temporal evolution as well. In our case, when executing the hydrocode, before running RLOS, we adjust the temporal density of snapshots, to be saved to disk at regular intervals. The smaller those intervals, the better the temporal resolution of hydrocode data. A series of snapshots shall then be loaded to RAM by RLOS, which therefore requires a multiple quantity of memory, in order to run properly, than the hydrocode itself. Time is measured in simulation time units, which are read by PLUTO's attached 'pload.pro' routine, which loads data into RLOS.

The total time span available to a LOS, $\Delta t_{LOS(total)} = t_{(last-shot)} - t_{(first-shot)}$ [1] (as measured in simulation time units, *not* merely in number of snapshots), should be preset to be larger than the light crossing time of the model system, at the selected LOS angle settings. Documenting the model jet evolution generally requires hydrocode data saves to be rather dense in time, especially for fast-changing flows. On the other hand, a lower temporal resolution will probably suffice for a steadier, slower-paced flow.

[1] Not to be confused with the interval Δt_{shot} between *successive* snapshots

6.4.2. Traversing the 4D arrays

Introduction. A series of hydrocode snapshots are loaded to RAM, populating the elements of 4-dimensional (4D) arrays. From a *temporal* point of view, we begin from the simulation time corresponding to the first of the loaded snapshots, called shotmin. From a *spatial* point of view, we start at the first point of the imaging plane, which is a side of the computational box (Figure 13). As the calculation advances, in 3D space, along the LOS being drawn (Figure 14), the algorithm keeps checking whether to jump to a new *temporal* slice, while staying 'on target' in 3D (Figure 15). Consequently, the LOS advances in time, through data (Figure 16), by accessing succesive instants from the 4D data arrays.

Time-resolved imaging calculations. For every LOS, there is a point of origin (POO), located on the "imaging side" of the computational grid (Figure 13). That point, addressed in the code as (nx10, ny10, nz10) and here as O′, is the beginning of the LOS's axes x′, y′, z′, parallel to x, y, z respectively. A 2D loop covers the imaging surface, the POO successively locating itself at each of the latter's points.

As we progress along a LOS, a record is kept of where we are, in 3D space. This record comprises the LOS's own integer coordinates, rc, uc, and cc, measured, in cells, from its POO. The above symbols stand for right-current, up-current and climb-current, representing the current LOS advance in the x′, y′ and z′ axes, respectively (Figures 13 and 14). The current ray position is then (nx10+rc, ny10+uc, nz10+cc).

A timer variable, curtime (standing for current LOS time), is introduced for each LOS, recording the duration of insofar ray travel along the LOS. The aforementioned timer is preset at the beginning of each LOS, to the hydrocode time of the first loaded data snapshot.

We then proceed to calculate the current length of the LOS

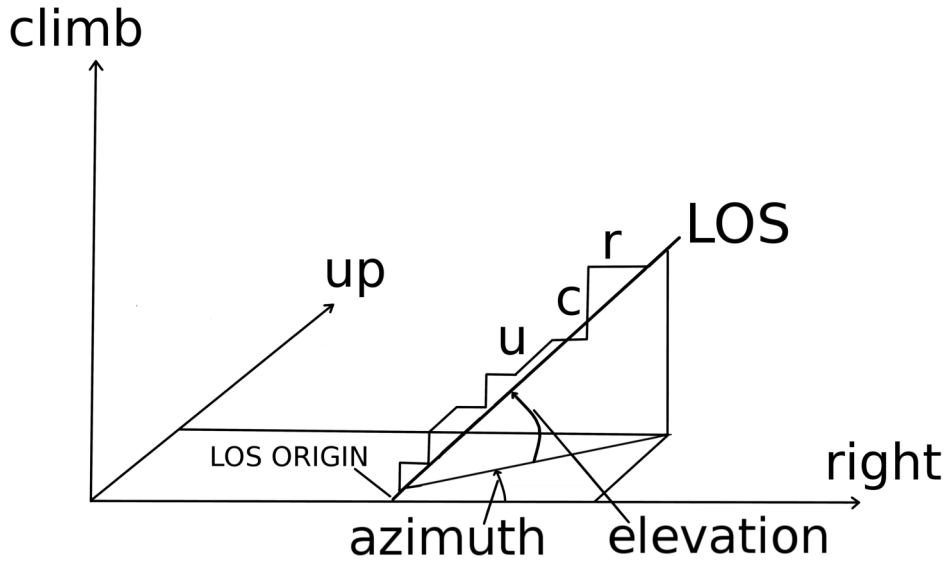

Figure 14: A schematic of the spatial propagation of the line of sight (LOS) through the 3D Cartesian computational grid. In the discrete grid, according to the design of the algorithm, there are 3 available directions to be taken at each step along the LOS: *right*, *up* and *climb*. These correspond to x, y and z, respectively. During propagation, the LOS 'tries' to follow its given direction, as defined by the two angles of azimuth and elevation. More specifically, every two steps a decision if first made on azimuth, either right or up. Then, for elevation, it is either climb, or another azimuth decision. In the Figure, along the LOS, horizontal steps point to the 'right' direction. Diagonal steps represent going 'up', while vertical ones constitute 'climb' steps.

$$l_{los(current)} = [(dlr * (nx1current - nx10))^2 + (dlu * (ny1current - ny10))^2 + (dlc * (nz1current - nz10))^2]^{1/2} \quad (42)$$

where the LOS length is measured in cell length units and

$$nx1current = nx10 + rc,\ ny1current = ny10 + uc,\ nz1current = nz10 + cc \quad (43)$$

Along the x, y and z directions, dlc, dlu, dlr are the respective *normalized* hydrocode cartesian cell lengths. Their values are usually unity, or close to unity, as set in the hydrocode by the user, and RLOS requires them fixed,

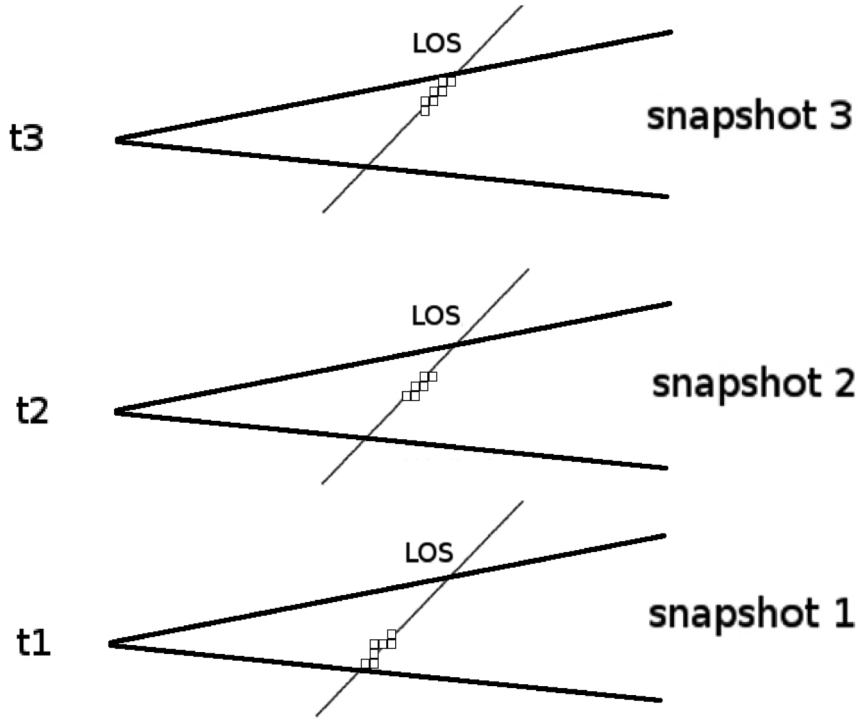

Figure 15: Three successive instants of a line of sight traversing a jet. At regular intervals, we jump to a new 3D slice of a 4D spacetime array, obtaining a discrete approximation of the time continuum, in the form of hydrocode snapshots.

meaning only homogeneous grids are currently supported. Furthermore, if the hydrocode grid is read, by pload, at a reduced resolution, then RLOS cell sizes are automatically adjusted accordingly.

We can finally write

$$l_{los(current)} = [((dlr * rc)^2) + ((dlu * uc)^2) + ((dlc * cc)^2)]^{1/2} \tag{44}$$

We then proceed to calculate curtime, the current hydro simulation time of the light ray along the LOS.

$$curtime = l_{los(current)}/c_{light} + t_{0(LOS)}. \tag{45}$$

485 $t_{0(LOS)}$ is the timestamp of the first loaded snapshot, when the LOS begins to be drawn, from its point of origin, and clight is the speed of light, in cells per simulation second.

When curtime exceeds the next snapshot's timetag, the algorithm switches

to drawing the LOS through the 3D volume of the next available snapshot (Figure 15). We keep moving along the same LOS in 3-D space, but we have just shifted to a new instant in the time records of the hydrocode. The above temporal shift is repeated as many times as required by the relevant criterion along the LOS, until the spatial end of the LOS.

6.4.3. Aiming the line of sight

The direction of a LOS in 3D space is defined by the two angles of azimuth (angle 1) and elevation (angle 2) (Figure 13), where the plane of angle 1 is the x′y′ plane, parallel to xy. For a jet parallel to the y axis, the angle between the local jet matter velocity $\vec{u}$, and the LOS, losu=$(\widehat{L\vec{O}S}, \vec{u})$, is usually small, when angle 1 approaches 90 degrees, and vice versa (Figure 17). As is well known [19], the angle losu affects the relativistic emission calculations.

Short of jet precession occuring, the plane of angle 2 (elevation) is largely perpendicular to the jet when angle 1 is zero, while it is roughly parallel to the jet when angle 1 is 90 degrees. Usually, the jet bears an approximate cylindrical symmetry, meaning that for a small angle 1, by varying angle 2, we 'rotate' the view around the jet axis, producing similar intensities throughout the way. In summary, for a jet moving along the y axis, the smaller angle 1 is, the less difference varying angle 2 makes.

On the other hand, for angle 1 nearing $\pi/2$, varying angle 2 rotates the view within a plane approximately parallel to the jet, resulting to considerable differences. Consequently, the larger angle 1 is, the stronger the effect, on the synthetic image, from changing angle 2.

6.5. Frequency-shift

SOS these refer only to EM rad. Not to particles, aka neutrinos.

Radiation emitted at a given frequency, from fast-moving jet matter, is taken to be Doppler shifted in frequency

$$f_{obs} = f_{calc} D \tag{46}$$

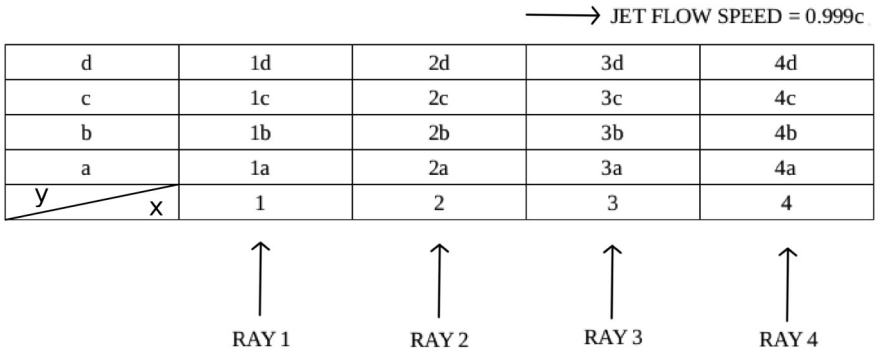

TIME	1	2	3	4
RAY 1	1a	-	-	-
RAY 2	2a	1b	-	-
RAY 3	3a	2b	1c	-
RAY 4	4a	3b	2c	1d

Figure 16: Simultaneous advance, in both space (2D) and time, of a few lines of sight. Top half depicts the spatial situation at t=1. Sixteen jet matter portions currently occupy this mini 4 by 4 grid. Each piece of matter is named after its position at t=1 and retains that name as it moves along. The bottom half shows how the situation evolves as time marches on, with light rays meeting different jet segments that cross their path. A dash means a light ray meeting jet matter other than the above, or nothing at all.

where f_{obs} is the observed frequency and f_{calc} is the frequency used in the emission calculations, performed in the jet frame of reference [19]. In order to accomodate for the shift, a power-law spectrum, falling off with frequency, is employed

$$S_{obs(f)} \propto f^{-\alpha} \tag{47}$$

with α assumed, as an approximation, to take the value of $\alpha = 2.0$, generally referring to the optically thin region of the jet. For D $\geq$ 1, emission is calculated at a frequency lower than the observed, resulting to a higher intensity, since the spectrum employed generally decreases with frequency.

Alternative frequency shift. RLOS may include different emission dependencies on frequency, where we calculate intensity at f_{calc} and observe that at f_{obs}.

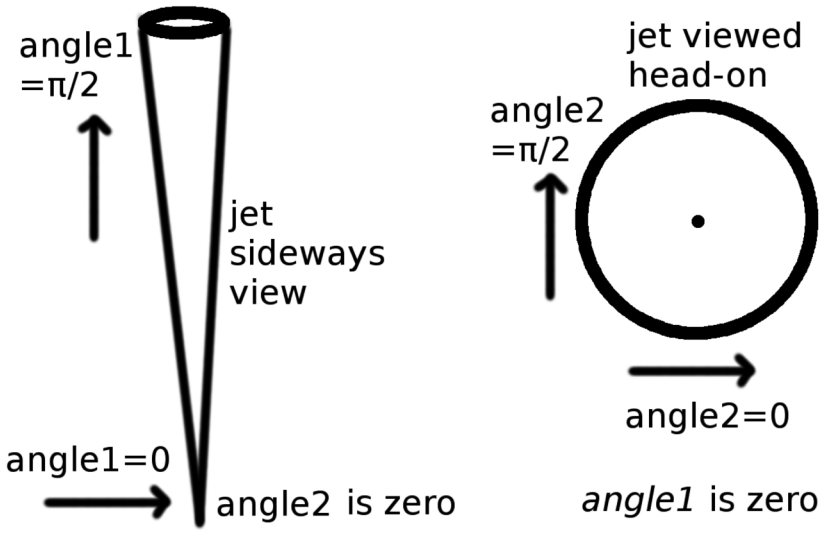

Figure 17: The geometric arrangement with regard to the viewing angles in the model, for the special cases of angle2 = 0 (left) and angle1 = 0 (right). For each sub-case, the arrow shows the direction of the LOS, which is different than the reader's direction of view.

SUPER SOS 290319 ref2 here and generally clarify OBS vs JET. Also, consider Cawthorne's 1991 page 199 simple syncrotron jet model. as a concrete example for a user spectrum SOS.

At the moment, the above is included only as a quantitative indicator, where intensity may be optionally multiplied by the square of the ratio $f_{calc}/f_{obs} = 1/\mathrm{D}^2$, partially negating the effect of Doppler boosting.

7. RLOS210

141119 We now have finished RLOS version 2.10. It includes a unified, functionalized, modular approach. Both XZ and YZ versions have now been unified, for both focused beam amd also parallel LOS's. Latest tests as suggested at the start of this paper draft! Also, we add some description to this paper fo the new version. Code completely re-written now!

****

****

131119 RLOS 2.10 code description.

Make this also into a new section in the rlos paper.

This is the latest version of rlos. Version 2 is a major upgrade of the original rlos code. This time the program is broken up into procedures and functions, with a modular structure.

The program allows the user to select which case to simulate, through an external parameter file rlos_params_v245.txt. There is a unified approach, where the same modules operate on different geometries, through parameterization.

The user may select the values of the parameters of rlos version 1, and fully employ them. As menitoned above, there is no more a different version of rlos for XZ and YZ plane image formation. Now, there is one version of the code for both cases. Furthermore, for each of those cases the user may select either radiograph or camera obscura imaging tachnique.

Radiograph has all Lines of Sight parallel to each other, just like rlos v.1. This means the film (fiducial imaging screen) is the size of the scene (grid), like an X-ray medical image. The latter type of image shows clearly the various details of the system.

On the other hand, camera obscura, or focused beam, has a focal point, where the eye of the fiducial observer is located. The imaging screen, in camera obscura, is also of varied size: It may be equal, or smaller to the grid slice, at a given point along either x or y axis, depending on YZ or XZ imaging plane case. At the moment, the fiducial imaging screen must be parallel to the corresponding side of the grid, i.e. either XZ or YZ. Screen location on-axis may vary within the grid. The smaller the screen, the smaller the image.

The focal point may reside either on the side of the grid, or outside the grid, BUT within the limits of the projection of the XZ or YZ plane. It may have negative or zero axis position, but its two planar coords must be smaller than the grid size.

Direction angles are no longer necessarily constant throughout the calculation: for the focused beam case, each LOS is drawn with a different set of azimuth (phi1) and elevation (phi2) angles. Angles are calculated using the lines that connect the focal point and the imaging screen point, which is the target point for the LOS.

The LOS then begins from the focal point, if it resides on the grid side, or from the LOS entry point, calced suitably (here recent relevant calc, upgrade of bversion 2.10). From then on, it advances using aiming algos, trying to pass through the targeted screen point. It normally gets the target, or misses it closely! In general, the higher the resolution, the better the accuracy in this respect.

SOS for GR pseudo-Newtonian sim, logical next step is to introduce D(phi1), D(phi2), i.e. alter angles aALONG a LOS, from cell to cell, according to the effect of the potential.

Then, jet production may be imaged, if the hydrocode can employ external forces from a Kerr BHole.

SOS ADD A FIGURE HERE in the rlos paper version of this text.

7.1.1. Back in time integration along the LOS

In this version, calculations may be done either ahead in time, or backwards in time, from a selected time instant (tpicked) backwards. For camera obscura, back in time is generally the correct way to proceed. For radiograph, ahead in time also works fine, assuming a suitable fiducial setup of the jet system vs the observer. tpicked is only employed when back in time switch is activated in the external param file. tpicked must be generally towards the end of the pre-selected range of dump files, or timeshots, to be loaded to RAM. Suffcient backwards time range must be provided, for the LOS to travel back through time without reaching the beginning of the gris. Else, code cannot finish integration along LOS. When testing, the facility of altering light speed, from rlos1, may be used to play and study this effect.

Pathfinding algos have been upgraded for this version. For each combination

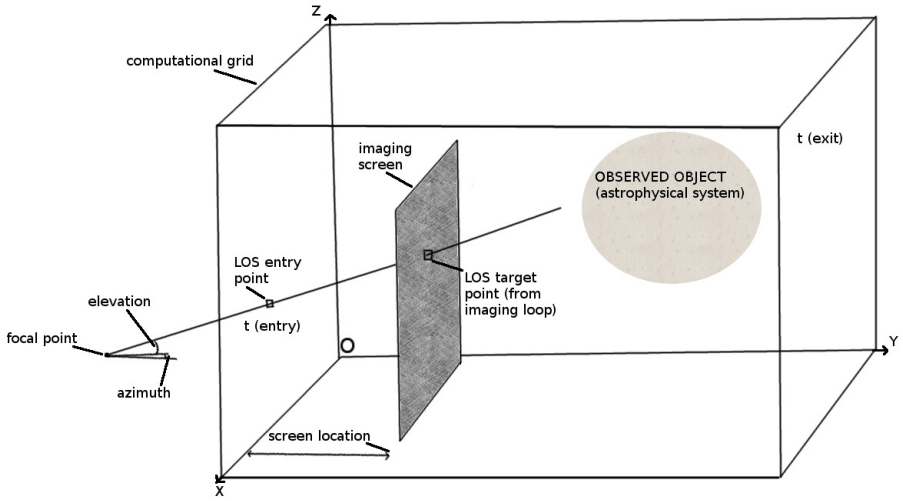

Figure 18: First and only part of the first batch of the results.

of XZ or YZ and radiograph or camera obscura, a certain set of such pathfinders are employed.

141119 figures do: a 3D-geometry figure (inclding the screen, the focal point, the focused beam, the old one is radiograph, this one shall be fbeam, also XZ vs YZ basics do include in this fig), a back-in-time figure, a block diagram of the functions SOS important.

SOS also do a figure for rlos2.10 externalparams like a table not figure

ADD THE FIGURES INTO THE PAPER OF RLOS1 but do a new section and a new version of the paper. From that paper, draw and do the 3-4 pgs new paper.

TBContinued

****

****

171119 tpicked is a param read from external param file! CAREFUL HERE! clarify we now set tpicked to t(shotmax)! We hare NOT USING tpicked any moar! SOS! $tpicked_fun = t_fun(shotmax_fun)$

Figure 19: A flow diagram of rlos2.1, depicting the procedures and functions called during program execution. A separate sub-diagram is provided for the main subroutine that draws the LOS.

161119 SOS erased, circa line 5000, the re-opening of param file!

610 **********

NEMISS comment, also applies here indirectly!

071119 it works!!! we have the following: lxi's: the same x and z between rlos and nemiss. vi's: OPPOSITE (x of rlos is z of nemiss and vice-versa) phi1,phi2 the same from rlos to nemiss aaaaafun: OPPOSITE z and z among 615 rlos and nemiss cccccfun:the same SO we did a 'reverse' function for aaaaa and there we reversed vx and vz. We then also created a coslosureverse which finally

MATCHED rlos's one!

Do tidy up here and make it nice

Parameter/Scenario	C (run3)	D (run4)	Comments
cell size ($\times 10^{10} cm$)	0.40	0.40	PLUTO's computational cell
ρ_{jet} (cm^{-3})	1.0×10^{11}	1.0×10^{14}	jet's matter density
ρ_{sw} (cm^{-3})	1.0×10^{11}	1.0×10^{12}	stellar wind density
ρ_{adw} (cm^{-3})	1.0×10^{11}	1.0×10^{13}	accretion disk wind density
t_{run}^{max} (s)	1.5×10^{3}	1.5×10^{3}	model execution time
Method	P. L.	P. L.	Piecewise Linear
Integrator	Ch. Tr.	Ch. Tr.	Characteristic Tracing
EOS	Ideal	Ideal	Equation of state
n	0.1005	0.1005	E_γ=100 GeV normalisation
BinSep (cm)	4.0×10^{12}	4.0×10^{12}	Binary star separation
$M_{BH}/M_\odot$	3-10	3-10	Mass range of collapsed star
$M_\star/M_\odot$	10-30	10-30	Mass range of Main Seq. star
$\beta = v_0/c$	0.26	0.26	Initial jet speed
L_k^p	10^{36}	10^{39}	Jet kinetic luminocity
grid resolution	300*500*300	300*500*300	PLUTO grid resolution (xyz)

Table 1: Scenario C (run 3) has artificially accelerated precession, while scenario D (run 4) has all the densities of the system increased by a few orders of magnitude, in order to account for a higher jet-mass flow-rate (jet's kinetic luminosity). The parameter n refers to a 'normalization' process that equates the results of two different methods of γ-ray emission calculations, one applied for energies above E_γ=100 GeV, and the other below this limit.

Parameter/Scenario	C (run3)	D (run4)	Comments
cell size SOS VERIFY ($\times 10^{10} cm$)	0.40	0.40	PLUTO's computational cell
VERIFY ρ_{jet} (cm^{-3})	1.0×10^{11}	1.0×10^{14}	jet's matter density
ρ_w (cm^{-3})	1.0×10^{11}	1.0×10^{12}	wind density
ρ_{dw} (cm^{-3})	1.0×10^{11}	1.0×10^{13}	VERIFY disk wind density
t_{run}^{max} (s)	1.5×10^{3}	1.5×10^{3}	model VERIFY run time
Method VERIFY	P. L.	P. L.	Piecewise Linear
Integrator VERIFY	Ch. Tr.	Ch. Tr.	Characteristic Tracing
EOS VERIFY	Ideal	Ideal	Equation of state
VERIFY BinSep (cm)	4.0×10^{12}	4.0×10^{12}	Binary star separation
$M_{BH}/M_{\odot}$	3-10	3-10	VERIFY Mass range of collapsed star
$M_{\star}/M_{\odot}$	10-30	10-30	D CONSIDER Mass range of Main Se
$\beta = v_0/c$	0.866 SOS 0.26	0.26	Initial jet speed
L_k^p	10^{36}	10^{39}	S Jet kinetic luminocity
grid resolution CORRECT THIS	300*500*300	300*500*300	PLUTO grid resolution (xyz)

Table 2: Table of run data